The International Journal of Advanced Manufacturing Technology
https://doi.org/10.1007/s00170-024-14887-9

ORIGINAL ARTICLE

A high-speed camera-based measurement system for monitoring and controlling the induced jet break-up fabrication of advanced ceramic breeder pebbles

Miao Zhang[1] · Oliver Leys[2] · Markus Vogelbacher[1] · Regina Knitter[2] · Jörg Matthes[1]

Received: 2 September 2024 / Accepted: 1 December 2024

Abstract
The production of lithium-rich ceramic pebbles is crucial for future fusion reactors, as they are one of the most important components of the tritium-breeding blankets. In order to produce high-quality pebbles, a melt-based fabrication process KALOS (KArlsruhe Lithium OrthoSilicate) has been developed at the Karlsruhe Institute of Technology (KIT), which produces pebbles utilising the break-up of a molten laminar jet. Since the production of the pebbles is very precise (with diameters of hundreds of micrometres) and significantly influenced by process parameters, a system that monitors and regulates the fabrication in real-time is essential. This paper elaborates on a high-speed camera-based measurement system for automatically monitoring and controlling the production process. Experimental proof demonstrates that the presented measurement system can provide the real-time sizes, locations and distance distribution of the molten ceramic droplets accurately. In addition, the system is also designed to enable the control of the pebble production by adjusting a production parameter, i.e. the driving frequency, based on the real-time output of the proposed measurement system.

Keywords Ceramic sphere manufacturing · Fusion energy · Jet break-up · Image processing · Melt-based process

1 Introduction

In the last several decades, nuclear fusion has attracted a spate of interest as a sustainable energy source for future generations on account of its safety and the limited amount of long-term radioactive waste. For nuclear fusion, one crucial step is the production of the two fuel components (deuterium and tritium), whereby deuterium can be extracted from seawater. In contrast, tritium must be generated on-site to ensure the reactor's self-sufficiency, allowing it to operate in a steady-state mode. For the purpose of generating the required tritium, lithium-rich ceramic pebbles are proposed to be installed into the wall of the fusion reactor in the form of pebble beds in so-called solid breeder blankets [1, 2]. Highly energetic neutrons, which are released during the fusing of tritium and deuterium, collide with the ceramic pebbles and cause the lithium to transmute into helium and tritium. Subsequently, the tritium is processed and rerouted back to react with deuterium.

In order to meet the demand for tritium breeding ceramics, a large number of processing techniques for the production of tritium breeders have been developed worldwide. For example, Lulewicz and Roux produced pebbles by applying

Miao Zhang and Oliver Leys contributed equally to this work.

✉ Oliver Leys
oliver.leys@kit.edu

Miao Zhang
miao.zhang@kit.edu

Markus Vogelbacher
markus.vogelbacher@kit.edu

Regina Knitter
regina.knitter@kit.edu

Jörg Matthes
joerg.matthes@kit.edu

[1] Institute for Automation and Applied Informatics, Karlsruhe Institute of Technology, Hermann-Von-Helmholtz-Platz 1, 76344 Eggenstein-Leopoldshafen, Baden-Württemberg, Germany

[2] Institute for Applied Materials, Karlsruhe Institute of Technology, Hermann-Von-Helmholtz-Platz 1, 76344 Eggenstein-Leopoldshafen, Baden-Württemberg, Germany

Published online: 18 December 2024

an extrusion-spherodisation technique [3]. A successful fabrication of Li_2TiO_3 pebbles using a slurry droplet wetting method is detailed in the study conducted by Park et al. [4]. Cai et al. [5] proposed a piezoelectric micro-droplet jetting approach to prepare Li_2TiO_3 green pebbles, which are then sintered. Hoshino developed a pebble production process based on an emulsion method [6] and even 3D printing has been proposed for the fabrication of tritium breeding structures [7].

At the Karlsruhe Institute of the Technology (KIT), the KALOS process was developed to produce advanced ceramic breeder pebbles using the break-up of a molten laminar jet and the subsequent solidification using liquid nitrogen [8, 9]. The pebbles are composed of lithium orthosilicate with a second strengthening phase of lithium metatitanate and are regarded as the solid EU-reference material for tritium breeding [1]. Advantages of the melt-based process include the scalability of the process, which is essential to be able to meet the demands for future reactors, and crucially, the ability to recycle the pebbles after use without the need for any wet-chemical processing [10]. Compared to the previously used melt-spraying process [11], the break-up of a laminar jet offers an increased control of the generated droplet size and therefore a higher control of the resulting solidified pebble size distribution.

The efficiency of the breeder blankets, and therefore of the fuel cycle, is dependent on a high pebble packing factor to maximise the bulk lithium density. At KIT, pebbles are produced in a size range of 250 to 1250 µm; a range that is expected to provide a high packing factor in the complex geometries of the breeder blankets. The break-up of the jet in the KALOS process occurs due to Plateau-Rayleigh instabilities growing on the surface of the jet until the surface tension forces overcome the viscous forces and a droplet breaks off [12, 13]. In general, the instabilities arise from random ambient disturbances, but recently, the process has been adapted to allow the application of selected driving frequencies to the system to control the break-up of the jet and thereby control the size distribution of the produced pebbles. This has resulted in higher process yields and an increase in the degree of monodispersity of the produced pebbles [14].

In order to investigate and quantify the jet break-up characteristics, a system using a high-speed camera and accompanying image processing algorithm was developed [15]. For the sake of quantifying the regularity of the jet break-up, an index referred to as the coefficient of variation (CV) was introduced that denotes the normalised standard deviation of the droplet spacing. A small CV value indicates a regular and stable jet break-up with a high degree of monodispersity. By modulating the disturbance frequency on the jet, it is possible to lower the CV value, resulting in a more stable and regular jet break-up to ensure the production of pebbles within the desired size range. This study investigates the limits of the range of frequencies that have a beneficial effect on the break-up of the jet and a feedback mechanism is implemented to the process control to ensure a low CV value.

This contribution aims to present a high-speed camera-based measurement system that can monitor, as well as control the production of ceramic pebbles, in real time. The paper is organised as follows: Sect. 2 introduces the fabrication procedure of the ceramic pebbles as well as the theoretical foundation of the jet break-up. The complete measurement system is illustrated in Sect. 3, including the high-speed camera system, image processing algorithms (for instance, jet detection and droplet identification) for determining and monitoring the process, and the jet break-up driving frequency control concept. Section 4 presents and discusses the results of the introduced measurement system. Section 5 concludes the paper.

2 Advanced fabrication of ceramic pebbles

The ceramic pebbles are produced by the KALOS process based on the break-up of a molten laminar jet. The section provides an introduction to the advanced pebble fabrication process and the theoretical foundation regarding the jet break-up.

2.1 Fabrication process

Starting powders are pre-reacted to form a powder with a composition of 70 mol% Li_4SiO_4 and 30 mol% Li_2TiO_3, which is then filled into a platinum alloy crucible inside a furnace. Figure 1 shows a schematic of the process set-up. The crucible is then heated up in a furnace to approximately 1400 °C to form a melt. A pressure of 320 mbar is applied to the crucible to force the melt through a small nozzle (300 µm diameter) on the underside, thereby forming a laminar jet. The jet then breaks up into droplets, which exit the furnace and enter a cooling tower, where they are solidified using liquid nitrogen. The pebbles are then collected at the base of the tower and transferred to the laboratory for characterisation. An example of the produced pebbles can be seen in Fig. 1 (right). Figure 1 also presents an example image recorded by the high-speed camera in the middle. As proved by the image, the camera system can capture the droplets clearly, which forms the basis of the measurement system described in the next section. For this study, focus was also placed on the sizes and size distribution of the produced pebbles (i.e. the solidified droplets), which would allow a comparison with the results from the image processing. These measurements were performed with a particle analyser "HAVER CPA 2–1" by Haver & Boecker, Germany.

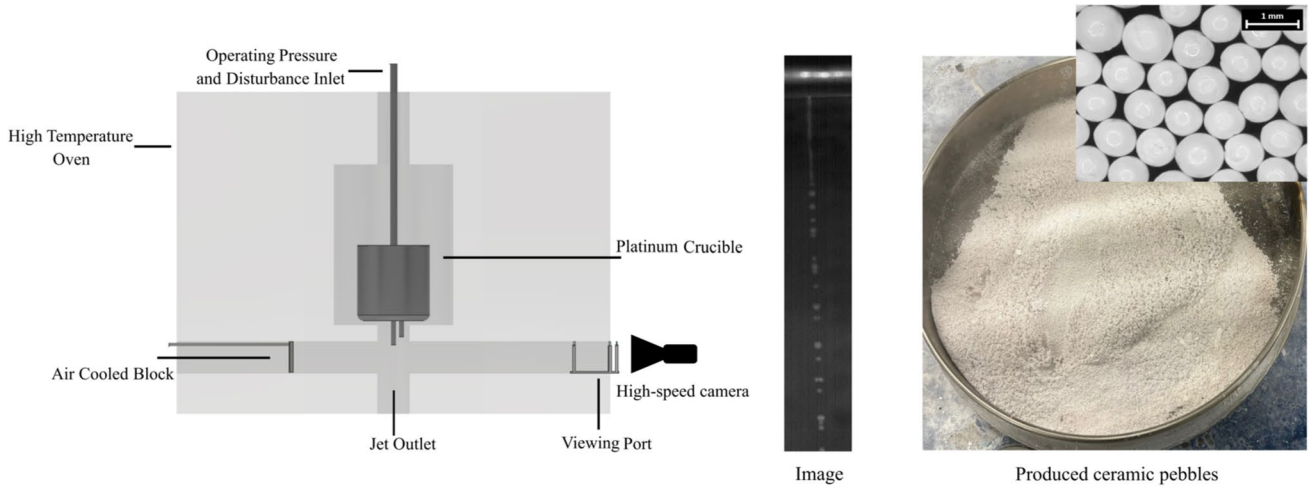

Fig. 1 High-temperature KALOS production experimental set-up and the gathered pebbles

2.2 Jet break-up theory

The break-up of the molten jet occurs due to the growth of so-called Plateau-Rayleigh instabilities. These are disturbances that grow on the surface of the jet in the shape of sinusoidal waves and once the wave reaches a certain amplitude, the surface tension forces will overcome the viscous forces, causing a droplet to break off from the jet. In general, four parameters control the break-up of the jet. These are the dimensionless Weber and Reynolds Numbers specific to the fluid properties and jet speed, and then there are the disturbance relevant factors, namely the disturbance amplitude and the wavenumber applied to the jet [16]. As the fluid properties cannot be manipulated at the processing temperature and a suitable operating pressure (directly affecting the jet velocity) for a laminar jet was found in a past study [17], this just leaves the disturbance parameters as possible options for increasing the control of the jet breakup. According to Rayleigh's theory on the break-up of inviscid jets, disturbances will grow on the surface of laminar jets if the wavenumber k is between 0 and 1 [12]. Furthermore, an optimum wavenumber k_{opt} for the fastest growth of the disturbances can be found at a value of approximately 0.7 [12, 13].

$$0 < k = 2\pi r\frac{f}{v} < 1 \tag{1}$$

$$k_{opt} = \frac{2\pi r}{v} \bullet f_{opt} \approx 0.7 \tag{2}$$

At the KALOS process, disturbances are applied to the jet by vibrating the process pressure at selected driving frequencies to control the jet break-up/droplet generation. As both the jet velocity v and radius r remain constant during production, the applied frequency is directly correlated to the wavenumber, meaning that only frequencies within a certain range will have an effect on the jet break-up, with the presence of an optimum frequency f_{opt} (corresponding to k_{opt}) for the fastest growth of the disturbances. Within this range, the applied disturbances will suppress ambient disturbances (or noise) and lead to a more controlled and monodisperse jet break-up. At the optimum frequency, the disturbance waves will grow the fastest and result in the most monodisperse break-up possible, thereby giving the smallest CV value. The CV value is given by the normalised standard deviation of the droplet spacing:

$$CV = \frac{\sigma(s)}{\mu(s)} \tag{3}$$

where s is the droplet spacing.

3 Novel measurement system for monitoring and controlling the pebbles fabrication

In order to evaluate and control the droplet formation in real-time regarding the size of the generated droplets and the CV values, a framework has been developed that enables the real-time detection of the jet length, as well as the size and position of each produced droplet. As mentioned, the framework also allows the control of the driving frequency so that the CV value remains below a certain threshold. Figure 2 gives a schematic overview of the developed measurement system. As illustrated in the figure, the high-speed camera system captures images of the droplet formation directly at the nozzle. Afterwards, the framework evaluates

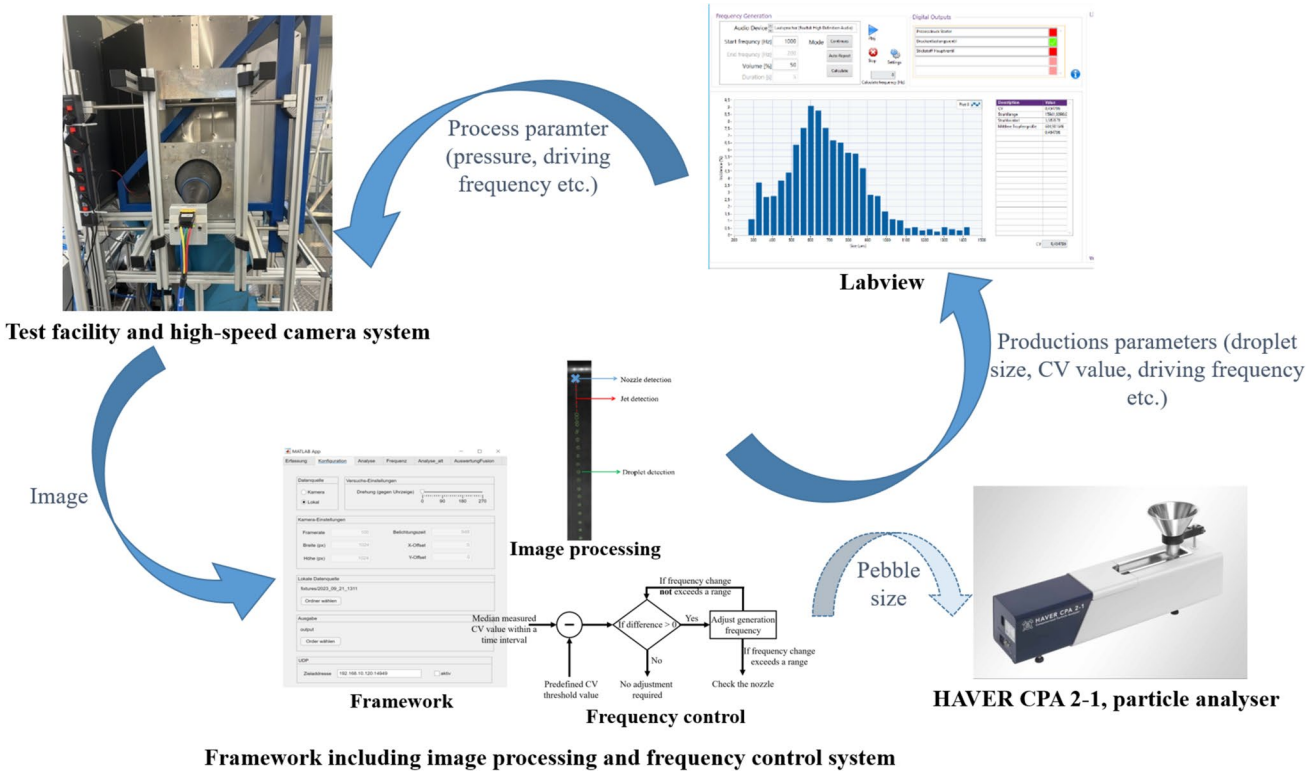

Fig. 2 Schematic of the novel measurement system

the production of the droplets based on image processing approaches. In accordance with the computed production parameters, the integrated control system regulates the driving frequency to ensure the production quality. The production parameters and control signal end up in the process control software, where parameters are visualised for intuitive monitoring of the production system. The control signal is passed to the hardware system for response. This online measurement system is connected with blue arrows in the figure. In addition, the system also has an offline system (marked by dashed arrows), which is used to analyse the size of the final collected ceramic pebbles and compare them with the results obtained from the online image processing for validating the proposed system. In the following, the corresponding hardware and approaches applied in the framework are detailed.

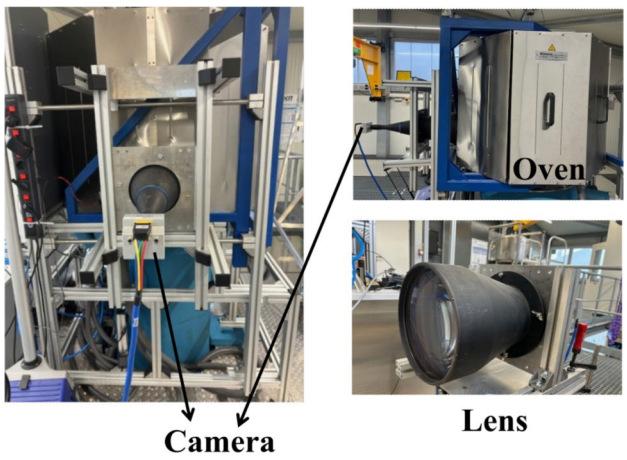

Fig. 3 High-temperature process furnace and mounted camera

3.1 Camera system

Figure 3 shows the real process set-up. As depicted in the figure, the camera and telecentric lens are mounted on the side of the high-temperature furnace. A port on the side of the furnace uses a combination of special glasses to allow the viewing of the droplet formation directly at the crucible nozzle. A cooled plate behind the jet provides sufficient contrast for the identification of the jet and droplets. The utilised high-speed camera (Optronis CP70-1-M-1000) can reach a frame rate of roughly 1000 frames per second (fps) with the maximum resolution of 1280×1024 pixels. By selecting a region of interest, the image size can be reduced, which results in a significantly increased maximum possible frame rate. The active area of the optical sensor is $8.448\ \text{mm} \times 6.758\ \text{mm}$ with a pixel size of $6.6\ \mu\text{m} \times 6.6\ \mu\text{m}$. The applied telecentric lens is a specially designed optical lens capable of maintaining a

constant magnification over a range of object distances. Thanks to the low aberration and constant magnification, the telecentric lens is ideal for use in scenarios that require high-precision dimensional measurements, such as the monitoring of the micron-sized droplets. According to the calibration, one pixel in image coordinates corresponds to a real size of approximately 71.94 µm × 71.94 µm.

The high-speed camera enables an exposure time as short as 2 µs, which allows for a clear recording of the rapid jet break-up processes and is also conducive to reducing the in-motion blurring. For the purpose of striking a balance between sufficient brightness of the droplets and keeping their shape spherical in the images, the exposure time was set to 160 µs. The detailed technical parameters of the utilised camera and lens are illustrated in Table 1. The camera captures the scene in the form of an image sequence containing temporally continuous images. The measurement system analyses the image sequence to compensate the fluctuation of individual image, which corresponds to a measuring cycle.

3.2 Image processing based monitoring system

The image sequence captured by the camera system in each measuring cycle is subsequently analysed by image processing approaches integrated in the framework. Figure 4 depicts the functions of the image processing–based monitoring system, including the detection of nozzle, jet and droplets. While the nozzle detection is only performed with the first image to enhance the computation efficiency, the detection of the jet and droplets takes place in all images within the sequence. Normally, an image sequence contains hundred images. As mentioned previously, the monitoring system ought to realise a real-time determination of the size and position of the individual droplets. In order to precisely localise the droplets and ignore the noise from the background, the nozzle and jet are detected first, which can

Table 1 Technical details of the high-speed camera and lens

Camera	Optronis CP70-1-M-1000	Lens	TC23172
Max. resolution	1280 × 1024 px	Working distance	526.9 mm
Framerate for max. resolution	1040 ps	Depth of field	159.2 mm
Framerate for 1/4 max. resolution	3800 ps		
Pixel size	6.6 µm		
Exposure time	2 µs up to 1/frame rate		

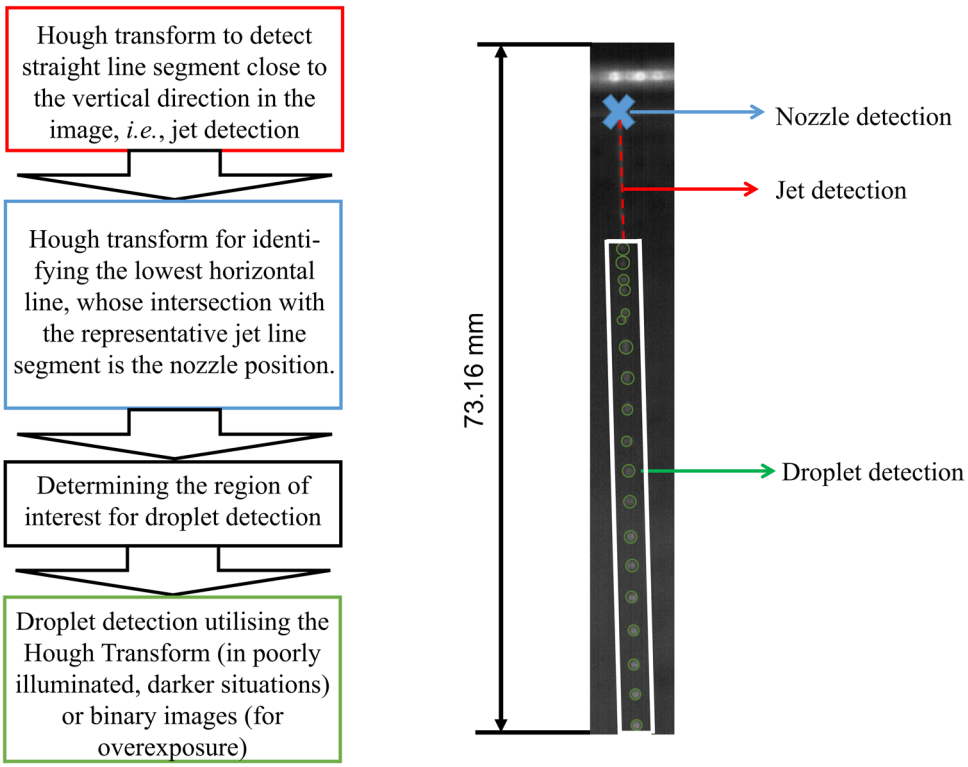

Fig. 4 Schematic of image processing tasks

constrain the search region of the droplets. Only droplets in the vicinity of the jet extension (region of interest) are detected, which prevents a large amount of non-droplet detection from the background and thereby speeds up the processing to ensure the real-time simultaneous detection of droplets. The region of interest is defined as a parallelogram, whose top and bottom sides are horizontal lines. The top line is at the end of the jet, while the bottom line is at the end of the entire image. The left and right sides are parallel to the detected jet and staggered by a certain pixel distance on the left and right, as illustrated by the white parallelogram in Fig. 4. In our study, the jet is considered to be a straight line with an angle of up to 10° to the vertical direction and is detected with the help of the Hough transform [18]. The location of the nozzle defines the start of the jet. To ensure accuracy, the nozzle is identified as the intersection of the line representing the jet with an upper, approximately horizontally oriented line representing the nozzle plate. The jet line portion that is above the intersection is then omitted. After determining the location of the jet and nozzle, the region of interest can be qualified and droplets within this region are detected by the Hough transform or binary image, which also allows the diameters of droplets to be determined.

As previously explained, the Hough transform is an important component of the monitoring system. The Hough transform is a feature extraction technique that finds instances of objects by a voting procedure carried out in a parameter space [18]. Initially, the Hough transform concerns the detection of lines in images and is therefore, adequate for the detection of the jet. With the development of the technique, the classical Hough transform has been generalised to identify arbitrary shapes, such as circles [19], and is also used for the detection of the droplets. In comparison to detecting droplets based on binary images, the Hough transform shows a better performance with respect to robustness and accuracy due to its relative insensitivity to individual pixel grey values. However, the accuracy of localising the detected shapes using the Hough transform greatly depends on their regularity. When the detected shape deforms for various reasons, e.g. exposure time, the Hough transform is biased in its localisation, which can significantly impact the present application for jet and droplet detection and thus the determination of the CV value. Therefore, the framework also has an alternative function that detects droplets based on binary images for special cases. For droplet detection based on binary images, each captured image is binarised by the Otsu threshold selection method [20] that performs automatic image thresholding corresponding to the grey value distribution of the image. The choice of method in practical applications depends on the exposure time. The system switches to this alternate method when the necessary exposure time is greater than 500 µs. According to Eq. 6, the CV value is the standard deviation of the droplet spacing ($\sigma(s)$) divided by the average spacing ($\mu(s)$). At first, all the detected droplets are rearranged from top to bottom according to their positions, then the distance between neighbouring droplets are calculated and noted as s_i, where i represents the ith droplet spacing of the N spacing. For each image, the CV value is calculated as:

$$\sigma(s) = \sqrt{\frac{1}{N-1}\sum_{i=1}^{N}\left(s_i - \mu(s)\right)^2} \tag{4}$$

and $\mu(s)$ is computed as:

$$\mu(s) = \frac{1}{N}\sum_{i=1}^{N} s_i \tag{5}$$

Since the monitoring system outputs the average CV value of an image sequence to reduce the result fluctuation, the real CV output is represented as:

$$\sigma = \frac{\sum_{j=1}^{M}\sigma(j)}{M} \tag{6}$$

where M denotes the amount of images within the image sequence. To assess the accuracy and adequacy of the monitoring system, the system was first tested on the break-up of a water jet at room temperature (using 100 mbar to form a jet through a 300 µm nozzle). Thereafter, it was applied to the KALOS process to quantify the generation of molten ceramic droplets and to illustrate the robustness and adequacy of the measurement system.

3.3 Control concept

Although in theory, all frequencies within a certain range should increase the regularity of the jet break-up (i.e. reduce the CV value), past work has shown that there are often irregularities in the response of the CV value to the driving frequency [14]. Within the effective frequency range, often the CV value will suddenly increase at certain frequencies. It is assumed that at these frequencies resonances develop in the system, which then lead to a more irregular break-up of the jet. If the CV value exceeds a predefined threshold, the driving frequency needs to be adjusted. The schematic of the process control is depicted in Fig. 5. A positively deviating CV value from the threshold indicates that the current driving frequency is inadequate to produce droplets that meet the requirements. Under this circumstance, the driving frequency is altered by a small amount from the existing frequency. When the frequency changes in a specific direction and the CV value becomes smaller, the frequency will continue to move in this direction in small increments until the CV value is below the threshold again. In general,

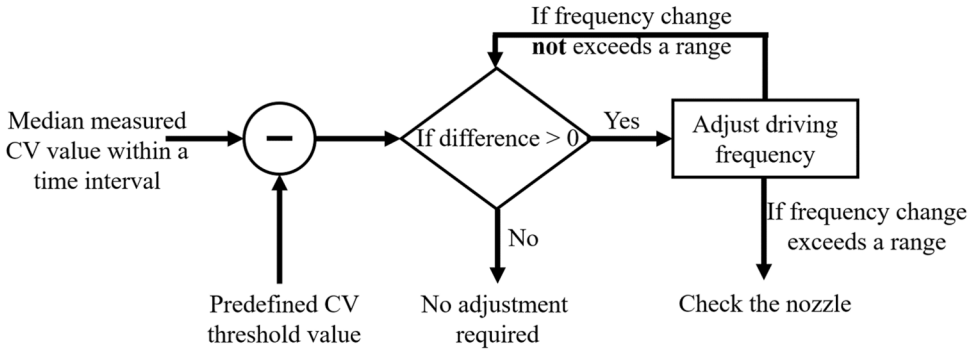

Fig. 5 Schematic of the process control

a particular process set-up is accompanied by several fixed optimal driving frequencies. Theoretically, the frequency only needs to change within a small range. When the frequency has been varied to a certain value, and the CV value is still unsatisfactory, the system will give an indication and recommend checking the nozzle for a possible disturbance or malfunction. In this case, the issue is most likely due to the wetting of the nozzle by the melt, thereby changing the jet characteristics (such as the diameter).

4 Results and discussion

Based on the measurement system demonstrated in the previous section, the crucial production parameters, i.e. the CV value and the diameter of individual droplets, can be monitored and controlled in real time. This section presents and discusses the experimental results. The image processing methods are applied to compute the CV values and diameters of water and molten ceramic droplets at different driving frequencies. Based on extensive experimental experience, as well as theoretical foundations, applying frequencies higher than 3000 Hz will not affect the break-up of the jet. As described in Sect. 2.2, Rayleigh's theory states that only frequencies within a certain range will influence the break-up of the jet [12]. Outside of this range (i.e. above 3000 Hz), no effect is to be expected. Therefore frequency ramps from 0 to 5000 Hz were used to study the effects of the frequency, while being sure to be cover the entire range of influence. Subsequently, certain frequencies were identified that could provide optimal results and were investigated.

4.1 Experimental effect of the driving frequency on the regularity of the water jet break-up

Figure 6 shows the images of the water jet break-up taken by the high-speed camera with a frame rate of 500 fps. Images taken at 500 Hz intervals are presented in the figure. In the experiment, the frequency increased uniformly from 0 to 5000 Hz over 3 min. Furthermore, the corresponding CV values as well as the diameters in µm computed by the image processing algorithms are displayed on the bottom. As illustrated by Fig. 6, the driving frequency has a significant influence on the CV values as well as on the diameters of the droplets produced.

As the frequency increases, the CV value grows slightly first. When the frequency reaches 1000 Hz, the break-up of the water jet becomes very regular, leading to a very small CV value. Subsequently, with further increasing the frequency, the production of water droplets again turns irregular and the CV value varies between 0.4 and 0.7. Meanwhile, the size of the water droplets also fluctuates slightly with the frequency. At the frequency of 1000 Hz, the CV value reaches a minimum within all the presented frequencies. At this frequency, the diameter of the water droplets is also the smallest, which indicates the fastest growth of the disturbances ($\approx f_{opt}$) and corresponds to the lowest CV value. Outside of this frequency, the diameters of the water droplets vary roughly around 500 µm.

4.2 Experimental effect of the driving frequency on the regularity of the molten ceramic jet break-up

Figure 7 presents the appearance of the molten ceramic jet break-up using different driving frequencies and utilising the same camera settings as in Sect. 4.1. With the gradual increase in frequency, the average diameter becomes larger and then smaller. The change in the CV value, on the other hand, is difficult to infer from the figure precisely. Nevertheless, as indicated by Fig. 7, the smaller the CV value, the shorter the corresponding jet length. This coincides with the theory from Sect. 2, which describes a theoretical range of influence for the driving frequency. As illustrated by Fig. 7, the smallest CV value occurs at the driving frequency of around 1000 Hz. Compared to the water droplets, the produced molten ceramic droplets trigger a smaller CV value and a larger droplet radius on average, most likely due to the different fluid properties.

Results from the image processing algorithm are shown in Fig. 8 a and b, where the horizontal coordinates represent the driving frequency and the vertical coordinates represent

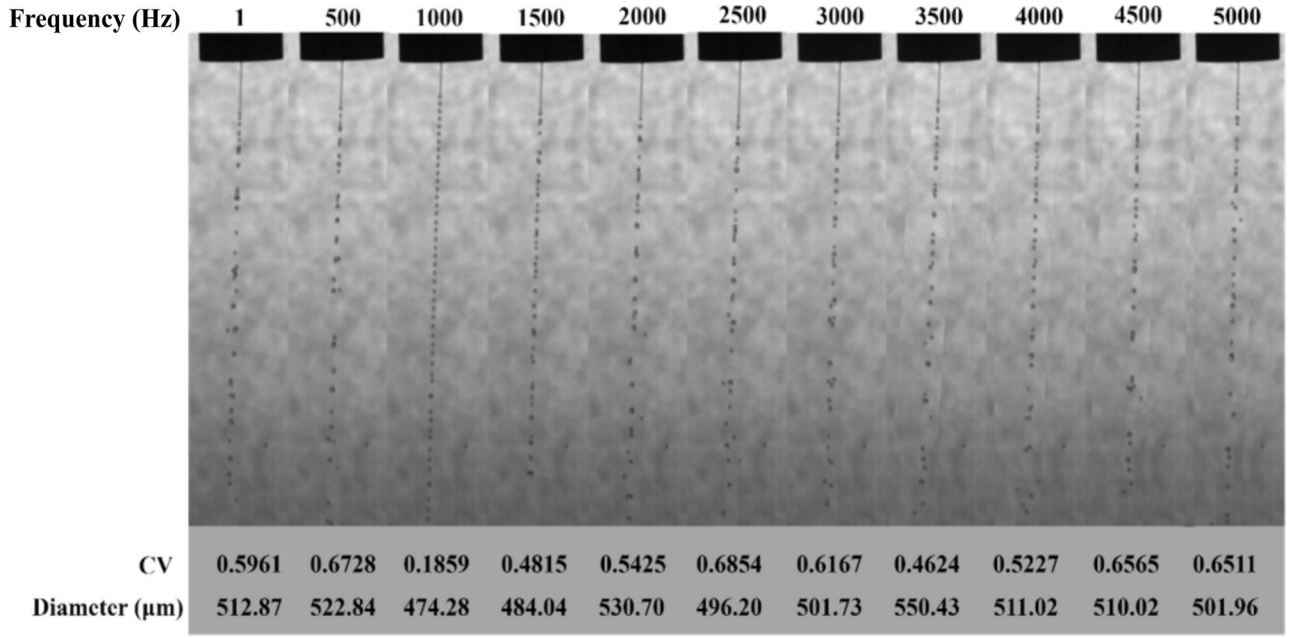

Fig. 6 Effect of the driving frequency on the appearance of produced water droplets

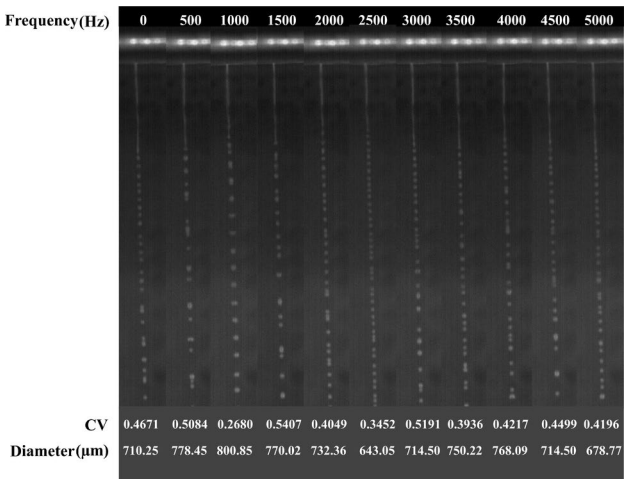

Fig. 7 Effect of the driving frequency on the appearance the molten ceramic jet break-up

the CV and diameter, respectively. The blue points inside the graph stand for the CV values or median diameter values corresponding to each frequency (frame), while the black lines in the graph are smoothed data via robust linear regression [21] over a window of 200 frames. Figure 8 clearly shows that frequencies between roughly 800 Hz and 2600 Hz have an effect on the break-up of the jet. According to the theory, there should be a continuous range of frequencies that influence the jet break-up, with a certain frequency leading to the lowest CV value. However, the presence of suspected resonances in the system is clear from Fig. 8. After a reduction in the CV value after about 800 Hz, it starts to increase again at about 1100 Hz up to the starting CV value, after which it drops again after about 1800 Hz. This results in two minima: one at about 1000 Hz and one at about 2300 Hz. At frequencies between these two minima, it seems the jet break-up is disturbed by internal resonances. This corresponds to the images of the irregular jet break-up for 1500 Hz and 2000 Hz in Fig. 7.

Figure 8 b shows that the droplet diameter can be controlled to a certain extent within the effective range. At a driving frequency of 1000 Hz, droplets with diameters of about 750 μm are formed and at 2500 Hz, 550 μm droplets are formed. The diameter also appears to decrease linearly between these two sizes. Again, the presence of resonances in the system can be seen at about 1500 Hz, where there is a larger amount of variation around the smoothed data value.

The results show that the smallest CV occurs at the driving frequency of approximately 1000 Hz. Therefore, we selected 1000 Hz as the driving frequency set-point for a test batch and studied the droplet generation and resulting pebble sizes at this frequency. The results are presented in Figs. 9 and 10. We present the probability density function of the CV value and diameter in a histogram with an approximated normal distribution in Fig. 9, where the black dashed lines stand for the values with the highest probability density and the red dashed lines represent the average values of the normal distributions. As shown in Fig. 9, for the recorded sequence, the average CV value obtained at 1000 Hz is 0.062, and the majority of the CV values are below 0.2, with only a tiny percentage of CV values exceeding 0.2.

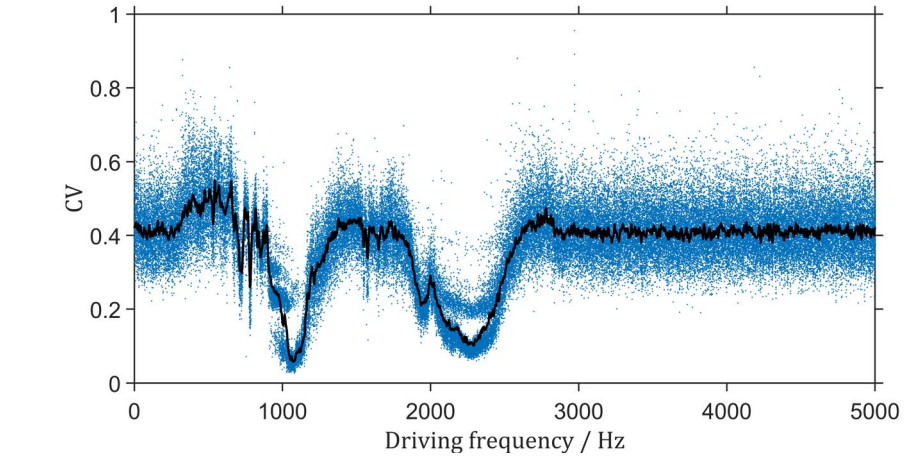

(a)

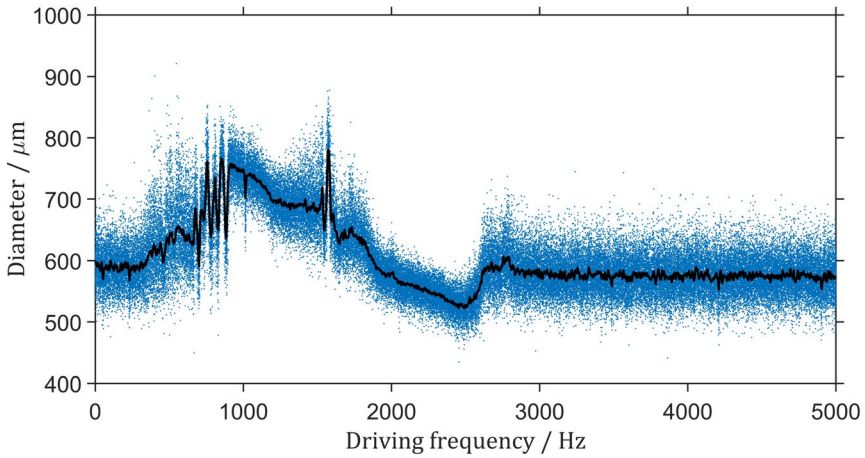

(b)

Fig. 8 Effect of the driving frequency on **a** the CV value and **b** the median diameter of the droplets

With respect to the droplet diameter, the diameter distribution in intervals of 5 µm is represented by a blue histogram. The diameter with the highest probability occurs in the interval 760 to 765 µm. The average and variance of the diameter distribution are also calculated, based on which a fitted normal distribution is shown in red with a mean value of 732.05 µm. The vast majority of the produced droplets are between 500 and 1000 µm in diameter.

In order to validate the adequacy and accuracy of the proposed measurement system, the solidified pebbles were collected and physically analysed to derive their sizes and distribution, as shown in Fig. 10. A histogram with a larger interval represents the distribution of the pebble diameters. Meanwhile, the cumulative distribution is marked with a red line. According to the analysis, the diameters of the pebbles are concentrated between 600 and 800 µm. The highest probability diameter is around 750 µm. This fits to the size of the generated droplets as seen in Fig. 9b. The secondary and tertiary peaks (at 950 µm and 1075 µm) correspond to the diameters generated when the volume of two or three primary droplets merge, respectively. About 90% of the droplets have diameters below 1000 µm. Although certain solidification effects will slightly change the size between the droplets and the solid pebbles, the results of the pebble size distribution and the image processing of the jet break-up are in high agreement with each other, thereby validating the system's accuracy. Moreover, the measurement system only monitors the droplet production within a limited area below the nozzle, while the pebbles are collected after the cooling stage of the process. As a consequence, the droplets may undergo slight physical deformation during their fall outside the monitoring range, leading to a difference between the two results.

In addition, we compared the droplets produced at 1000 Hz, and from 3000 to 5000 Hz (i.e. outside of the range of influence), as shown in Table 2. Apparently, droplets produced at 1000 Hz have a more uniform, symmetric distribution with fewer extremes. This is indicated by the

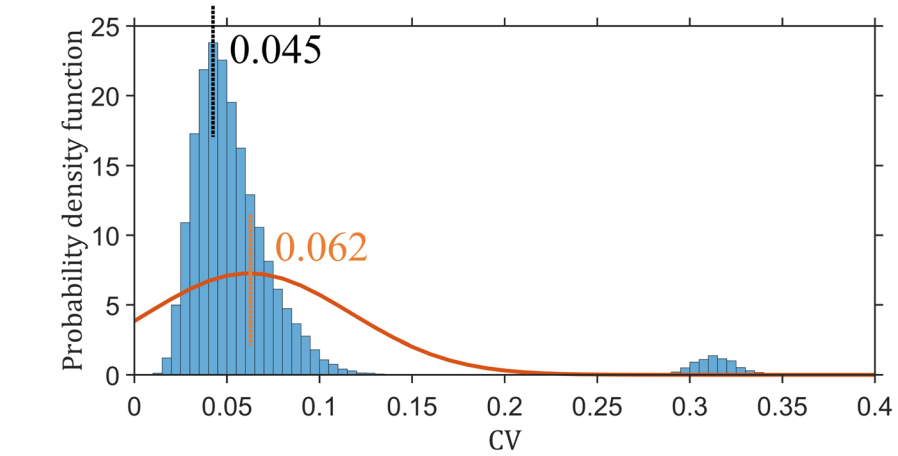

(a)

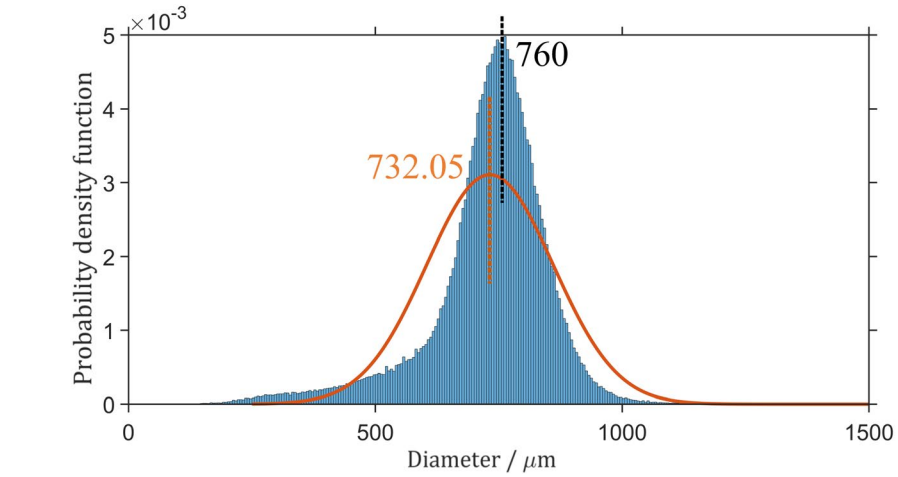

(b)

Fig. 9 Measured **a** CV value probability density distribution and **b** diameter distribution at the driving frequency of 1000 Hz

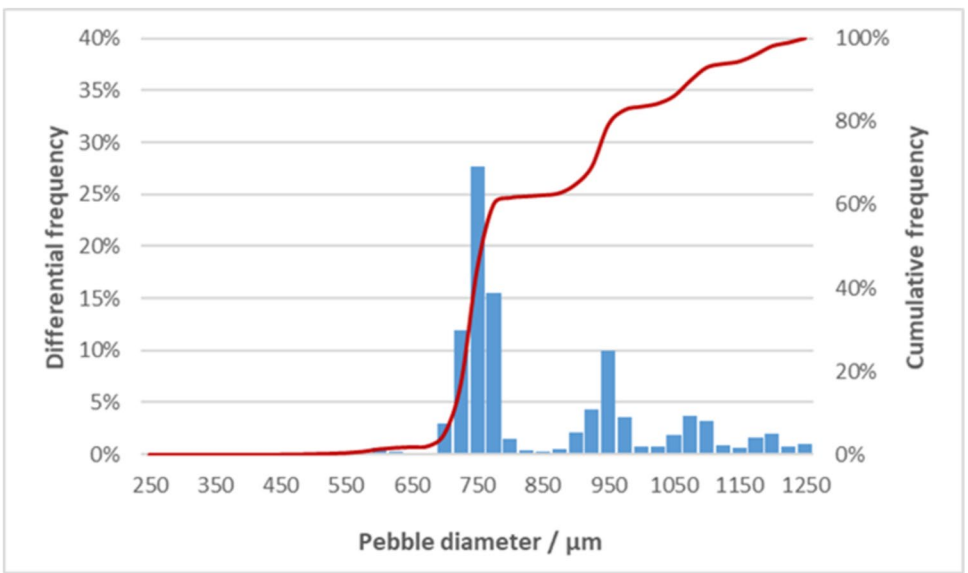

Fig. 10 Measured diameter distribution via physical analysis at the driving frequency of 1000 Hz

Table 2 Comparison of the droplets produced at 1000 Hz and 3000–5000 Hz

Frequency	1000 Hz	3000–5000 Hz
Average diameter in µm	720.02	592.07
Median diameter in µm	723.93	574.24
Variance	3323	29669

fact that (1) the mean and median droplet sizes are very close to each other at 1000 Hz, and (2) the variance is almost 10 times smaller in comparison to droplets produced at 3000 to 5000 Hz. This also demonstrates that, although the CV is a parameter based on the droplet spacing, it can characterise the regularity of the droplet sizes very well. Furthermore, the determination of the CV values allows a comparison of the results to the jet break-up theory. A clear range of influence could be identified for the melt-based process and, although apparent resonances in the system make it difficult to identify a single minimum, it can be seen that the degree to which the CV can be reduced also varies within the range. Although further work is needed to study the nature of the resonance effects, this phenomenon once again highlights the need for a control system to manage unknown system responses. Since the pebbles produced using unsuitable frequencies are very inhomogeneous in size, it is not possible meet the requirements for a standardised product for future fusion reactors, meaning a measurement system is necessary to ensure and improve the quality of the production process.

As shown in Fig. 9a, even though the CV values are already very concentrated at a low value with the fixed optimum frequency of 1000 Hz, several values still deviate significantly from this value. These inappropriate CV values are most likely due to measurement inaccuracies caused by various factors, such as unfavourable grey values of the droplets, and can strongly impact the real-time CV values based regulation system. Even though the actual production of ceramic pebbles meets the required conditions, the system will still adjust the production parameter based on these unreasonable measurements. Therefore, in our designed system, the process parameter, i.e. the driving frequency, is regulated in accordance with the median CV value over a particular time interval instead of each individual CV value. To determine the appropriate time interval, we computed the median CV values over 10, 50, 100 and 200 frames for the nozzle and present the outcome in Fig. 11. As shown in Fig. 11, the peak is clearly visible with a very small interval (10 frames), while when the interval grows to 50 frames, the peak almost disappears. Continuing to increase the interval to 100 frames, the median becomes very stable, fluctuating only within a small range. With further increasing the number of frames, the fluctuations are even smaller. Obviously, the smaller the selected interval, the better the system's dynamics. In this case, a suitable interval is set as 100 frames. Since the high-speed camera can reach a frame rate of thousand frames per second, the time occupied by 100 frames is only a few hundred milliseconds, which can fully meet the production requirements.

5 Conclusion

This paper introduces a real-time high-speed camera-based measurement system to monitor and control the production of lithium-rich ceramic pebbles to be used for nuclear fusion applications. The image processing based monitoring system enables a real-time analysis of the production outcomes by providing the diameter of the produced droplets and the normalised standard deviation of the droplet spacing (CV). The CV value is also the most

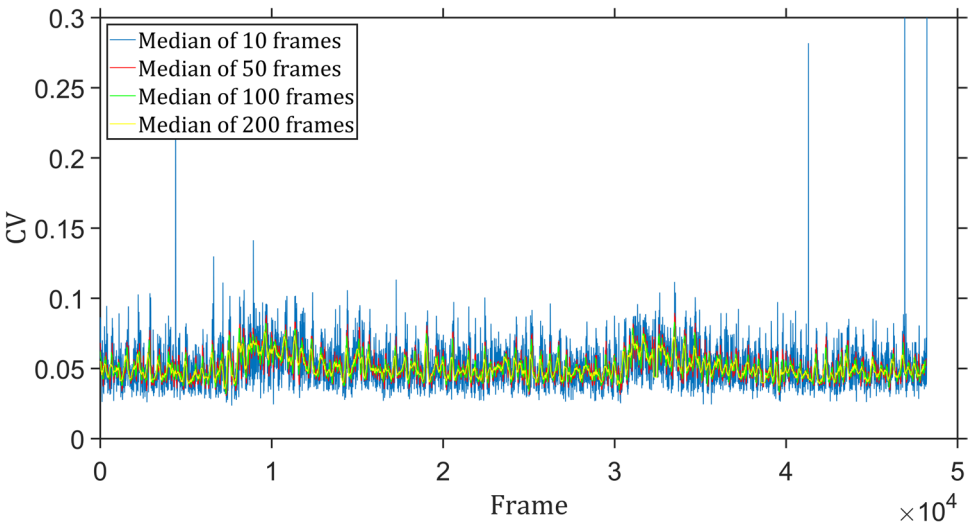

Fig. 11 Median CV value over different time intervals at the driving frequency of 1000 Hz

vital indicator for the droplet production, and in accordance with which, the driving frequency process parameter, ought to be adjusted. As indicated by the jet break-up theory in the second section, a small CV value represents a regular and stable jet break-up and is thus preferred for the production process. Thus, the measurement system is also designed to contain a control algorithm, which controls the driving frequency to ensure a satisfactory CV value. With the proposed system, we studied the impact of the driving frequency on the CV value and the droplet diameter. At first, experiments were conducted with a range of driving frequencies to get a preliminary global view of the water and molten ceramic droplet generation behaviour, whereby this research focuses mainly on the molten ceramic droplets. According to the outcomes, the driving frequency affects the production performance significantly within a certain range. Thereafter, the influence tends to be negligible. For the utilised nozzle, the optimal frequency is expected to appear at around 1000 Hz. Hence, this frequency is considered as an initial driving frequency for the process and was also investigated in detail subsequently. The results of the proposed measurement system were in agreement with an analysis of the final produced pebbles, thereby proving the adequacy and accuracy of the control system. Since the driving frequency is one of the most vital process parameters for controlling the droplet generation, the measurement system shows its necessity for choosing the initial frequency and for the further adjustment of the frequency.

Our experiments with the described settings indicate the adequacy of the proposed measurement system for monitoring and controlling the droplet generation in the pebble production process. With the proposed system, the quality of the produced ceramic pebbles can be ensured to meet the requirements of the further application in fusion reactors. Future research will investigate the performance of the designed control system under various conditions. Furthermore, the control system can also be designed to search for the local optimal frequency with acceptable adjustments to further improve the production process. Additionally, the robustness of the system by experiments with different process parameters, such as alternative nozzle diameters, should also be studied. Moreover, the image processing approach will be expanded to study the development and velocity of the generated droplets. The determination of the droplet velocity would allow an estimation of the process mass flowrate, which is also essential for the process control.

Acknowledgements This work has been carried out within the framework of the EUROfusion Consortium, funded by the European Union via the Euratom Research and Training Programme (Grant Agreement No 101052200 — EUROfusion). Views and opinions expressed are however those of the author(s) only and do not necessarily reflect those of the European Union or the European Commission. Neither the European Union nor the European Commission can be held responsible for them.

Author contributions All authors contributed to the study conception and design. Material preparation, data collection and analysis were performed by Miao Zhang and Oliver Leys. The first draft of the manuscript was written by Miao Zhang and Oliver Leys, and all authors commented on previous versions of the manuscript. All authors read and approved the final manuscript.

Funding Open Access funding enabled and organized by Projekt DEAL. This work has been carried out within the framework of the EUROfusion Consortium, funded by the European Union via the Euratom Research and Training Programme (Grant Agreement No. 101052200 — EUROfusion).

Declarations

Competing interests The authors have no relevant financial or non-financial interests to disclose.

References

1. Knitter R, Chaudhuri P, Feng YJ, Hoshino T, Yu I-K (2013) Recent developments of solid breeder fabrication. Fifteenth Int Conf Fusion React Mater 442:420–424. https://doi.org/10.1016/j.jnucmat.2013.02.060
2. Hernández FA et al (June2018) Overview of the HCPB research activities in EUROfusion. IEEE Trans Plasma Sci 46(6):2247–2261. https://doi.org/10.1109/TPS.2018.2830813
3. Lulewicz JD, Roux N (2022) Fabrication of Li_2TiO_3 pebbles by the extrusion–spheronisation–sintering process. J Nuclear Mater 307–311(Part 1):803–806. https://doi.org/10.1016/S0022-3115(02)00981-9
4. Park Y-H, Cho S, Ahn M-Y (2014) Fabrication of Li_2TiO_3 pebbles using PVA–boric acid reaction for solid breeding materials. J Nucl Mater 455:106–110. https://doi.org/10.1016/j.jnucmat.2014.05.027
5. Cai J, Xu G, Lu H, Xu C, Hu Y, Cai C, Suo J (2022) Preparation of tritium breeding Li_2TiO_3 ceramic pebbles via newly developed piezoelectric micro-droplet jetting. J Am Ceram Soc 105:3753–3764. https://doi.org/10.1111/jace.18320
6. Hoshino T (2016) Pebble fabrication of super advanced tritium breeders using a solid solution of $Li_{2+x}TiO_{3+y}$ with Li_2ZrO_3. Nuclear Mater Energy 9:221–226. https://doi.org/10.1016/j.nme.2016.05.004
7. Liu Y, Chen Z, Li J, Gong B, Wang L, Lao C, Wang P, Liu C, Feng Y, Wang X (2020) 3D printing of ceramic cellular structures for

potential nuclear fusion application. Addit Manuf 35. https://doi.org/10.1016/j.addma.2020.101348
8. Kolb MHH, Knitter R, Kaufmann U, Mundt D (2011) Enhanced fabrication process for lithium orthosilicate pebbles as breeding material. Fusion Eng Des 86:2148–2151. https://doi.org/10.1016/j.jnucmat.2018.05.010
9. Leys O, Leys JM, Knitter R (2021) Current status and future perspectives of EU ceramic breeder development. Fusion Eng Des 164. https://doi.org/10.1016/j.fusengdes.2020.112171
10. Leys O, Bergfeldt T, Kolb MHH, Knitter R, Goraieb AA (2016) The reprocessing of advanced mixed lithium orthosilicate/metatitanate tritium breeder pebbles. Fusion Eng Des 107:70–74. https://doi.org/10.1016/j.fusengdes.2016.04.025
11. Knitter R, Alm B, Roth G (2007) Crystallisation and microstructure of lithium orthosilicate pebbles. J Nucl Mater 367–370:1387–1392. https://doi.org/10.1016/j.jnucmat.2007.04.002
12 Rayleigh L (1878) On the instability of jets. Proc London Math Soc s1–10:4–13. https://doi.org/10.1112/plms/s1-10.1.4
13. Eggers J, Villermaux E (2008) Physics of liquid jets. Rep Progress Pyhsics 71. https://doi.org/10.1088/0034-4885/71/3/036601
14. Leys O, Waibel P, Matthes J, Knitter R (2019) Ceramic pebble production from the break-up of a molten laminar jet ILASS-Europe 2019: 29th Conference on Liquid Atomization and Spray Systems, Paris
15. Waibel P, Matthes J, Leys O, Kolb M, Keller H, Knitter R (2014) High-speed camera-based analysis of the lithium ceramic pebble fabrication process. Chem Eng Technol 37:1654–1662. https://doi.org/10.1002/ceat.201300769
16. Eggers J (1997) Nonlinear dynamics and breakup of free-surface flows. Rev Mod Phys 69:865–930. https://doi.org/10.1103/RevModPhys.69.865
17. Leys O, Waibel P, Matthes J, Kolb M, Keller H, Knitter R (2018) Characterisation of high-temperature jet break-up for ceramic sphere production. Int J Adv Manuf Technol 98:2311–2318. https://doi.org/10.1007/s00170-018-2378-y
18 Hart PE (2009) How the Hough transform was invented. IEEE Signal Process Magazine 26(no 6):18–22. https://doi.org/10.1109/MSP.2009.934181
19. Ballard DH (1981) Generalizing the Hough transform to detect arbitrary shapes. Pattern Recogn 13:111–122. https://doi.org/10.1016/0031-3203(81)900091
20. Otsu N (1979) A threshold selection method from gray-level histograms. IEEE Trans Syst Man Cybern 9(1):62–66. https://doi.org/10.1109/TSMC.1979.4310076
21. Andersen R (2008) Modern methods for robust regression, sage university paper series on quantitative applications in the social sciences. **07-152**:1654–1662